International Journal of Heat and Mass Transfer 52 (2009) 1412–1420

Contents lists available at ScienceDirect

International Journal of Heat and Mass Transfer

journal homepage: www.elsevier.com/locate/ijhmt

Analysis of NO formation in high temperature diluted air combustion in a coaxial jet flame using an unsteady flamelet model

K.W. Lee, D.H. Choi *

Department of Mechanical Engineering, Korea Advanced Institute of Science and Technology, Daejeon 305-701, Republic of Korea

ARTICLE INFO

Article history:
Received 28 November 2007
Received in revised form 6 June 2008
Available online 22 October 2008

Keywords:
High temperature air combustion
Turbulent nonpremixed flame
Flamelet model
NO formation
Coaxial jet

ABSTRACT

The high temperature diluted air combustion, which improves the flame stability while lowers the NO emission level, has been numerically investigated. The Favre-averaged Navier–Stokes equations are solved by a finite volume method of SIMPLE type that incorporates the laminar flamelet concept with the standard k–ε turbulence model. The NO formation is estimated by solving the Eulerian particle transport equations in a postprocessing mode. Calculations are performed for a coflowing jet flame for various conditions of inlet air temperature and oxygen concentration. A production rate analysis of elementary reactions reveals major paths for NO formation. When the oxygen concentration is high, the reaction zone is formed near the fuel nozzle and the NO formation by the thermal mechanism becomes dominant, due to the increase in flame temperature. On the other hand, when the oxygen concentration is low, the reaction is spread out more uniformly in the furnace. The NO formation by the prompt route is dominant compared to other routes especially when the air is diluted with nitrogen.

1. Introduction

Due to the rapid industrialization of the world, the energy consumption is increasing at an alarming rate. The growing energy consumption eventually leads to increased emission of greenhouse gases, CO_2 and pollutants, such as SO_x and NO_x. Regulations on pollutant emission have been toughened in recent years. To cope with this changing environment, new combustion technologies that would improve the combustion efficiency and reduce pollutant emission have evolved. Nitric oxides, among other pollutants, are contributors of the production of acid rain and photochemical smog. The high temperature diluted air combustion is a promising combustion technology that reduces NO_x emission. Preheating the inlet air increases the combustion intensity and thus extends the stable combustion region. The higher flame temperature, however, accompanies increased NO_x emission. By lowering the oxygen concentration in the air, the temperature distribution in the furnace can be made uniform and the NO_x emission is effectively reduced.

Many experimental studies in the literature [1–3] on the characteristics of high temperature diluted air combustion showed that it yields very low NO_x emission, low luminosity, higher flame stability, large flame volume and a more uniform temperature field. The literature on the computational side of the study is also extensive: Yuan and Naruse [4] obtained the combustion characteristics of a cross-jet flame with highly preheated diluted air, which were in line with those of experiment, by using a PDF/mixture fraction model with equilibrium chemistry. Comparative studies on various relatively simple turbulent combustion models may be found in Orsino and Weber [5] and Yang and Blasiak [6]. The NO formation for highly preheated air conditions was examined by using either empirical correlations [7,8] or a full chemistry approach in the methane–air laminar diffusion flame [9]. The detailed NO_x formation routes in turbulent combustion, however, have not been examined thoroughly at high temperature diluted air condition.

For accurate prediction of NO_x emission, the complex turbulent combustion process, including turbulence and chemistry interaction, needs to be adequately accounted for. Among many combustion models, the laminar flamelet model [10] is proven to be effective in predicting complex physical phenomena, such as detailed chemistry, formation of pollutants, by decoupling chemical reactions from the turbulent flow field. Until recently, most flamelet model approaches commonly neglected the unsteady effects, which may become substantial when the process is slow such as in the formation of NO_x. Pitsch et al. [11] showed, in their study on the turbulent hydrogen–air diffusion flame, that while the temperature and the concentration of chemical components were predicted accurately by the steady flamelet model, NO was overpredicted. The results were shown to improve if an unsteady model was used. Barths et al. [12] proposed a more general Eulerian particle flamelet model (EPFM) that solves an Eulerian particle transport equation for probability to find the multiple flamelets, and successfully obtained the NO_x and soot

* Corresponding author. Tel.: +82 42 869 3018; fax: +82 42 869 3210.
E-mail address: d-h-choi@kaist.ac.kr (D.H. Choi).

0017-9310/$ - see front matter © 2008 Elsevier Ltd. All rights reserved.
doi:10.1016/j.ijheatmasstransfer.2008.08.015

Nomenclature

$a_{p,k}$	Plank mean absorption coefficients for radiating species k
c_p, $c_{p,k}$	specific heat of mixture and species k at constant pressure
D	diameter of fuel nozzle
D_z	mixture fraction diffusivity
h_k	specific enthalpy of species k
I_n	probability of finding nth flamelet
k	turbulent kinetic energy
P_k	partial pressure of species k
$\dot{q}_{rad}$	radiative heat loss rate per unit volume
r	coordinate in radial direction
t	time
$Sc_{\tilde{Z}}$, $Sc_{\tilde{Z''^2}}$	Schmidt numbers
T	temperature
T_b	background temperature
u_j	velocity component in jth direction
x_j	coordinate in jth direction
Y_k	mass fraction of species k
Z	mixture fraction
Z''^2	mixture-fraction fluctuation

Greek symbols

χ	scalar dissipation rate
$\tilde{\chi}_{st}$	mean scalar dissipation rate conditioned on stoichiometric mixture
$\hat{\chi}_{st,n}$	surface averaged conditional scalar dissipation rate of nth flamelet
ε	dissipation rate of turbulent kinetic energy
μ_t	turbulent viscosity
ρ	density
σ_B	Stefan–Boltzmann constant
σ_t	turbulent Prandtl number
$\dot{\omega}_k$	chemical production rate of species k
ζ	enthalpy defect

Subscripts

n	nth flamelet particle
st	stoichiometry

Superscripts

$\bar{\phi}$	Reynolds-averaged (density-unweighted) property
$\tilde{\phi}$	Favre-averaged (density-weighted) property

formation in a gas turbine combustor. More recently, the model was applied to solve the low oxygen dilution combustion [13].

The primary objective of the present study is to develop an analysis procedure using the laminar flamelet model coupled with the EPFM and examine the detailed NO formation characteristics for the turbulent nonpremixed coaxial jet flame with the preheated diluted air. Each NO formation mechanism, i.e., thermal, prompt, or N_2O intermediate mechanism, is discussed using detailed chemical kinetics. The important elementary reactions for NO formation are scrutinized by the production analyses.

2. Numerical procedure

The analysis procedure in this section describes both the steady and unsteady flamelet models. The unsteady effects are taken into consideration in the postprocessing stage by using the Eulerian particle transport equations.

2.1. Flamelet equations

In laminar flamelets, all scalars are functions of the mixture fraction and scalar dissipation rate. Their balance equations for species k and energy for unit Lewis numbers of chemical species are written as

$$\rho\frac{\partial Y_k}{\partial t}-\rho\frac{\chi}{2}\frac{\partial^2 Y_k}{\partial Z^2}-\dot{\omega}_k=0 \tag{1}$$

$$\rho\frac{\partial T}{\partial t}-\rho\frac{\chi}{2}\left[\frac{\partial^2 T}{\partial Z^2}+\frac{1}{c_p}\frac{\partial c_p}{\partial Z}\frac{\partial T}{\partial Z}-\frac{\partial T}{\partial Z}\sum_{k=1}^{N}\left(1-\frac{c_{p,k}}{c_p}\right)\frac{\partial Y_k}{\partial Z}\right]+\frac{1}{c_p}\left(\sum h_k\dot{\omega}_k+\dot{q}_{rad}\right)=0 \tag{2}$$

Here, the scalar dissipation rate is defined as

$$\chi(Z)=2D_Z\left(\frac{\partial Z}{\partial x_j}\right)^2 \tag{3}$$

and Y_k is the mass fraction, T the temperature, ρ the density, c_p the specific heat, h_k the specific enthalpy, $\dot{\omega}_k$ the chemical production rate, $\dot{q}_{rad}$ the radiative heat loss, D_Z the mixture fraction diffusivity and Z the mixture fraction. To obtain the solution of the flamelet equation, the relation between the mixture fraction and the scalar dissipation rate is needed. Peters [10] has proposed a one-parameter function as

$$\chi(Z)=\frac{a_s}{\pi}\exp\left\{-2[\mathrm{erfc}^{-1}(2Z)]^2\right\} \tag{4}$$

where erfc^{-1} is the inverse of the complementary error function and a_s is the velocity gradient at the stagnation point. The equation may be rewritten in terms of the stoichiometic values

$$\chi=\chi_{st}f(Z)/f(Z_{st}) \tag{5}$$

For adiabatic flame condition with negligible radiative heat loss, the mass fractions of all chemical species and temperature are determined by the mixture fraction Z and stoichiometric scalar dissipation rate χ_{st}. When radiation is not negligible, an additional variable, i.e., the enthalpy defect ζ [14], is introduced:

$$\zeta=h-[h_o+Z(h_f-h_o)] \tag{6}$$

which is the difference between the actual enthalpy and the enthalpy for the adiabatic case. The radiation effects could be substantial in predicting NO formation [15]. Treating the radiative heat transfer within a turbulent flame in detail is computationally very expensive. To lessen the computational burden, the optically thin radiation model is incorporated in which the radiative loss rate per unit volume may be obtained as

$$\dot{q}_{rad}=4\sigma_B\left(T^4-T_b^4\right)\sum P_k a_{p,k} \tag{7}$$

where σ_B is the Stefan–Boltzmann constant and P_k is the partial pressure of species k. The Plank mean absorption coefficients $a_{p,k}$ for radiating species k are calculated from the curve fits in TNF workshop (http://www.ca.sandia.gov/TNF/radiation.html).

2.2. Equations for the flow field

The governing equations for the turbulent flow field are the Favre-averaged, continuity and Navier–Stokes equations coupled with the standard k–ε model for turbulence closure. A cell centered, colocated finite volume scheme of SIMPLE type is developed and used to solve these equations. The mixing of fuel and oxidizer in the turbulent flow field is described by the transport equations for the mean mixture fraction $\widetilde{Z}$ and its variance $\widetilde{Z}''^2$

$$\frac{\partial}{\partial t}\left(\bar{\rho}\widetilde{Z}\right)+\frac{\partial}{\partial x_j}\left(\bar{\rho}\tilde{u}_j\widetilde{Z}\right)=\frac{\partial}{\partial x_j}\left(\frac{\mu_t}{Sc_{\widetilde{Z}}}\frac{\partial\widetilde{Z}}{\partial x_j}\right) \tag{8}$$

$$\frac{\partial}{\partial t}\left(\bar{\rho}\widetilde{Z}''^2\right)+\frac{\partial}{\partial x_j}\left(\bar{\rho}\tilde{u}_j\widetilde{Z}''^2\right)=\frac{\partial}{\partial x_j}\left(\frac{\mu_t}{Sc_{\widetilde{Z}''^2}}\frac{\partial\widetilde{Z}''^2}{\partial x_j}\right)+2\frac{\mu_t}{Sc_{\widetilde{Z}''^2}}\left(\frac{\partial\widetilde{Z}}{\partial x_j}\right)^2-\bar{\rho}\tilde{\chi} \tag{9}$$

where the Schmidt numbers $Sc_{\widetilde{Z}}$ and $Sc_{\widetilde{Z}''^2}$ are chosen to be 0.7 and the mean scalar dissipation rate $\tilde{\chi}$ is modeled as

$$\tilde{\chi}=C_\chi\frac{\tilde{\varepsilon}}{\tilde{k}}\widetilde{Z}''^2,\quad C_\chi=2.0 \tag{10}$$

where $\tilde{k}$ is the turbulence kinetic energy and $\tilde{\varepsilon}$ is the dissipation rate of $\tilde{k}$.

The mean properties of the reacting mixture in the computational domain are then evaluated by convoluting the tabulated values in the flamelet library with the probability density functions

$$\tilde{\phi}=\int_{-\infty}^{\infty}\int_0^{\infty}\int_0^1\phi(Z,\chi_{st},\zeta)\widetilde{P}(Z,\chi_{st},\zeta)\,dZ\,d\chi_{st}\,d\zeta \tag{11}$$

The mixture fraction and scalar dissipation rate are assumed to be statistically independent, so that the presumed probability density functions can be constructed as

$$\widetilde{P}(Z,\chi_{st},\zeta)=\widetilde{P}(Z)\widetilde{P}(\chi_{st})\widetilde{P}(\zeta) \tag{12}$$

The probability density functions for the mixture fraction and the dissipation rate take, respectively, the forms of the β function and the logarithmic normal distribution while that for the radiation effect is of delta function form. The details are laid out in Refs. [10,14] and are not repeated here.

2.3. The Eulerian particle flamelet model (EPFM)

The following Eulerian particle transport equations are solved in the postprocessing stage for the species concentrations and NO_x formation:

$$\frac{\partial}{\partial t}\left(\bar{\rho}\widetilde{I}_n\right)+\frac{\partial}{\partial x_j}\left(\bar{\rho}\widetilde{I}_n\tilde{u}_j\right)=\frac{\partial}{\partial x_j}\left(\frac{\mu_t}{\sigma_t}\frac{\partial\widetilde{I}_n}{\partial x_j}\right) \tag{13}$$

where $\widetilde{I}_n(x,t)$ is the probability of finding nth flamelet at location $\vec{x}$ and time t. The model is capable of treating both parabolic and elliptic flows.

Different flamelet particles with specific initial conditions are transported through the flow field along different pathways. Following Barths et al. [12], the initial distribution of the particles in the flow field is prescribed as

$$\widetilde{I}_n=\begin{cases}1 & \text{if } \widetilde{Z}>Z_{st} \text{ and } \widetilde{T}<1800\,\text{K}\\ 0 & \text{otherwise}\end{cases} \tag{14}$$

The initial flamelet particles are placed close to the fuel inlet because the temperature there is low and the NO formation is negligible in the fuel rich stream. For multiple flamelet particles, the initialization region is divided into the equal number of subregions to which each flamelet particle is assigned. The initial probability of finding a flamelet is then equal to unity in its own subregion and zero elsewhere.

Flamelet history of each particle is different and is represented as the variation of scalar dissipation rate. The surface averaged conditional scalar dissipation rate is given as

$$\hat{\chi}_{st,n}=\frac{\int_V\widetilde{I}_n\bar{\rho}\tilde{\chi}_{st}^{3/2}\widetilde{P}(Z_{st})\,dV}{\int_V\widetilde{I}_n\bar{\rho}\tilde{\chi}_{st}^{1/2}\widetilde{P}(Z_{st})\,dV} \tag{15}$$

where the integration is performed over the whole computational domain. In each subregion, the flamelet equations are solved with $\chi_{st}=\hat{\chi}_{st,n}$. The mean scalar dissipation rate conditioned on stoichiometric mixture $\tilde{\chi}_{st}$ in Eq. (15) is modeled from Eq. (5) by assuming that χ_{st} and Z are statistically independent

$$\tilde{\chi}=\tilde{\chi}_{st}\int_Z f(Z)/f(Z_{st})\widetilde{P}(Z)\,dZ \tag{16}$$

Equating this with the modeled average scalar dissipation rate in Eq. (10), one obtains

$$\tilde{\chi}_{st}=\frac{C_\chi\frac{\tilde{\varepsilon}}{\tilde{k}}\widetilde{Z}''^2}{\int_0^1 f(Z)/f(Z_{st})\widetilde{P}(Z)\,dZ} \tag{17}$$

The flamelet particles released at time $t=0$ are dispersed by convection and turbulent diffusion in the combustion chamber. The Favre-averaged mass fractions of chemical species at $\vec{x}$ are calculated by

$$\widetilde{Y}_k(\vec{x},t)=\frac{\sum_n\int_0^t\widetilde{I}_n(\vec{x},t')\widetilde{Y}_{k,n}(\vec{x},t')dt'}{\sum_n\int_0^t\widetilde{I}_n(\vec{x},t')dt'} \tag{18}$$

This is a weighted average of all flamelet particles over the corresponding period. Here, $\widetilde{Y}_{k,n}(\vec{x},t')$ is the Favre-averaged mass fraction of species k for the nth flamelet particle:

$$\widetilde{Y}_{k,n}(\vec{x},t')=\int_0^1 Y_i(Z,\hat{\chi}_{st,n})\widetilde{P}(Z)\,dZ \tag{19}$$

where $Y_k(Z,\hat{\chi}_{st,n})$ is the flamelet profile of the unsteady flamelet equations with scalar dissipation rate corresponding to each flamelet history.

Having obtained the steady flamelet solutions, Eqs. (1), (2) and (13) with the surface averaged scalar dissipation rates (15) are solved in succession in a coupled manner. The steady-state results are used to provide the initial condition for this unsteady procedure. The initial mass fraction of species associated with the NO_x mechanism (N, NH, NH_2, NH_3, NNH, NO, NO_2, N_2O, HNO, CN, HCN, H_2CN, HCNN, HCNO, HOCN, HNCO, and NCO) is set equal to zero. The Favre-averaged mass fraction of species k at $\vec{x}$ and t' for the nth flamelet particle is then evaluated from Eq. (19). The calculation is carried out until all flamelet particles are transported away from the combustor. Finally, the species mass fractions $\widetilde{Y}_k$ are obtained from Eq. (18).

3. Results and discussion

3.1. Code validation

The numerical model outlined in the previous section is then tested against the Meier-flame because of its ample experimental data base [16]. The experiment was originally carried out at DLR in Stuttgart and also later at the Sandia National Laboratories. The details of the two data sets are compared and discussed in Meier et al. [17]. The flame was one of the test cases at TNF Workshop of 1998 and many different results of various modeling approaches are available at (http://www.ca.sandia.gov/TNF/

3rdWorkshop/TNF3.html). The fuel composition is 22.1% CH_4, 33.2% H_2 and 44.7% N_2 by volume. The mean velocity and temperature of the fuel at the nozzle exit are 42.2 m/s and 295 K while those for the coflowing air are 0.3 m/s and 292 K, respectively.

The calculation is performed for the axisymmetric domain that extends to $x/D = 120$ and $r/D = 30$. After thorough grid dependency tests, a 70×80 grid is found to be adequate to resolve the flow field. The GRI 3.0 chemical reaction mechanism, which consists of 325 elementary chemical reactions including the NO_x chemistry and contains 53 species, is adopted. The CHEMKIN-II and TRANFIT subroutines [18,19] are used to obtain the thermodynamic and transport properties of each chemical species.

The small Lewis number of hydrogen molecule makes the non-equal diffusion effects more pronounced in flames where hydrogen is a major species. However, it was shown, for instance, in Bergmann et al. [16] and Meier et al. [17] that the effects of non-unity Lewis number become important only in the region close to the fuel nozzle. The differential diffusion effect disappears as the distance from the fuel nozzle increases. In the present study, the calculation is performed under the assumption that the Lewis number is unity.

The temperature, mixture fraction and mixture-fraction fluctuation fields along the centerline are compared in Fig. 1. The results by Sanders (http://www.ca.sandia.gov/TNF/3rdWorkshop/TNF3.html), who used laminar flamelet including full differential diffusion and the GRI 2.11 chemical reaction mechanism, are also plotted in the figure for reference. The temperature and the mixture fraction obtained in the present study are in very good overall agreement with the measured data. The mixture-fraction fluctuation is somewhat larger than the experiment in the near field but closely follows the experimental data farther downstream. Radiation is seen to play an important role as the results obtained without the radiation effects grossly overpredict the temperature beyond the point of maximum temperature. The close agreement in the upstream region is presumably due to the fact that the diffusive transport of heat in this region is very large compared to the radiation.

Fig. 2 depicts the NO concentration along the centerline. Calculations have been performed with varying number of flamelet particles to show its effects. Although the results degrade in the downstream region, it is apparent that the unsteady calculation improves the results considerably over the steady model. Increasing the number of flamelet particles improves the results but no further improvement is achieved when it exceeds six. It is also observed in the figure that the NO concentration is wildly overpredicted unless the radiation effects are not properly taken into account. The discrepancy in the downstream region may be attributed to the overpredicted flame length. The longer flame length results in a higher temperature and mixture-fraction fields which are directly responsible for a higher NO prediction. Besides, the chemical mechanism adopted in the calculation may also have affected the NO prediction. The performance of a chemical mechanism varies with the combustion conditions, such as air temperature, strain rate, pressure, fuel dilution, and partial premixing [20–22]. The widely used GRI 3.0 mechanism has a tendency of overpredicting NO levels.

The major and minor species concentrations along the centerline are presented in Fig. 3. The OH concentration shown in Fig. 3(a) is grossly underpredicted by the steady flamelet model. The unsteady model, on the other hand, gives much better results when multiple flamelet particles are used. The CO concentration compared in Fig. 3(b) shows that the maximum value is slightly underpredicted by both the steady and unsteady models. Unlike in the case of NO or OH, the results appear to be insensitive to the number of flamelet particles. For major species, since the concentration distributions are not sensitive to the number of flamelet particles in the present calculation, only the results of six flamelet particles are presented in Fig. 3(c) and (d). The unsteady flamelet model performs slightly better than the steady model, but the difference appears to be negligible. The calculated results are gener-

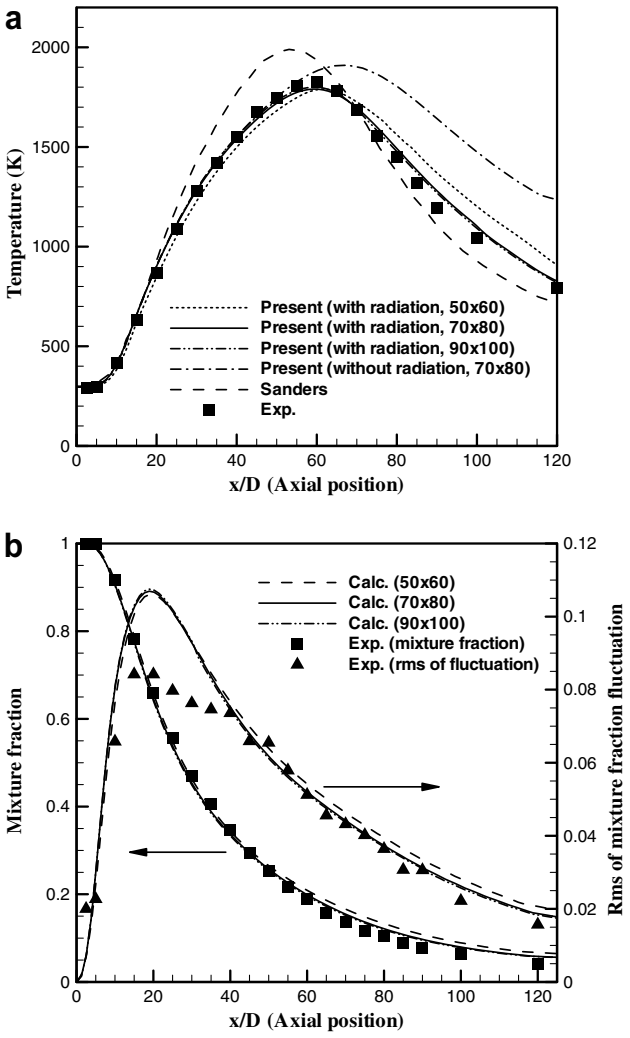

Fig. 1. Temperature, mixture fraction and RMS of fluctuation along the centerline: (a) temperature and (b) mixture fraction and RMS of fluctuation.

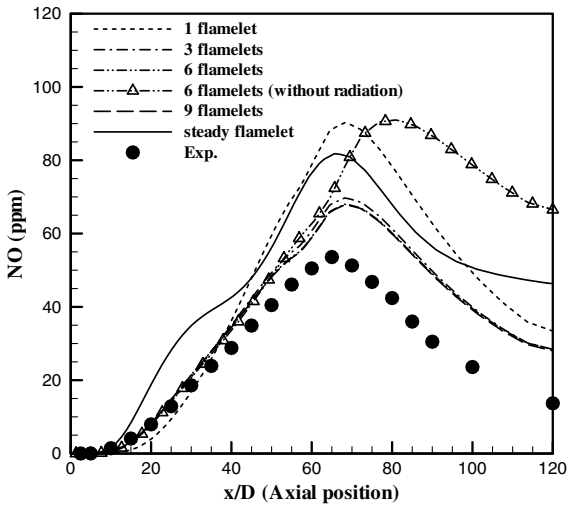

Fig. 2. NO concentration distribution along the centerline.

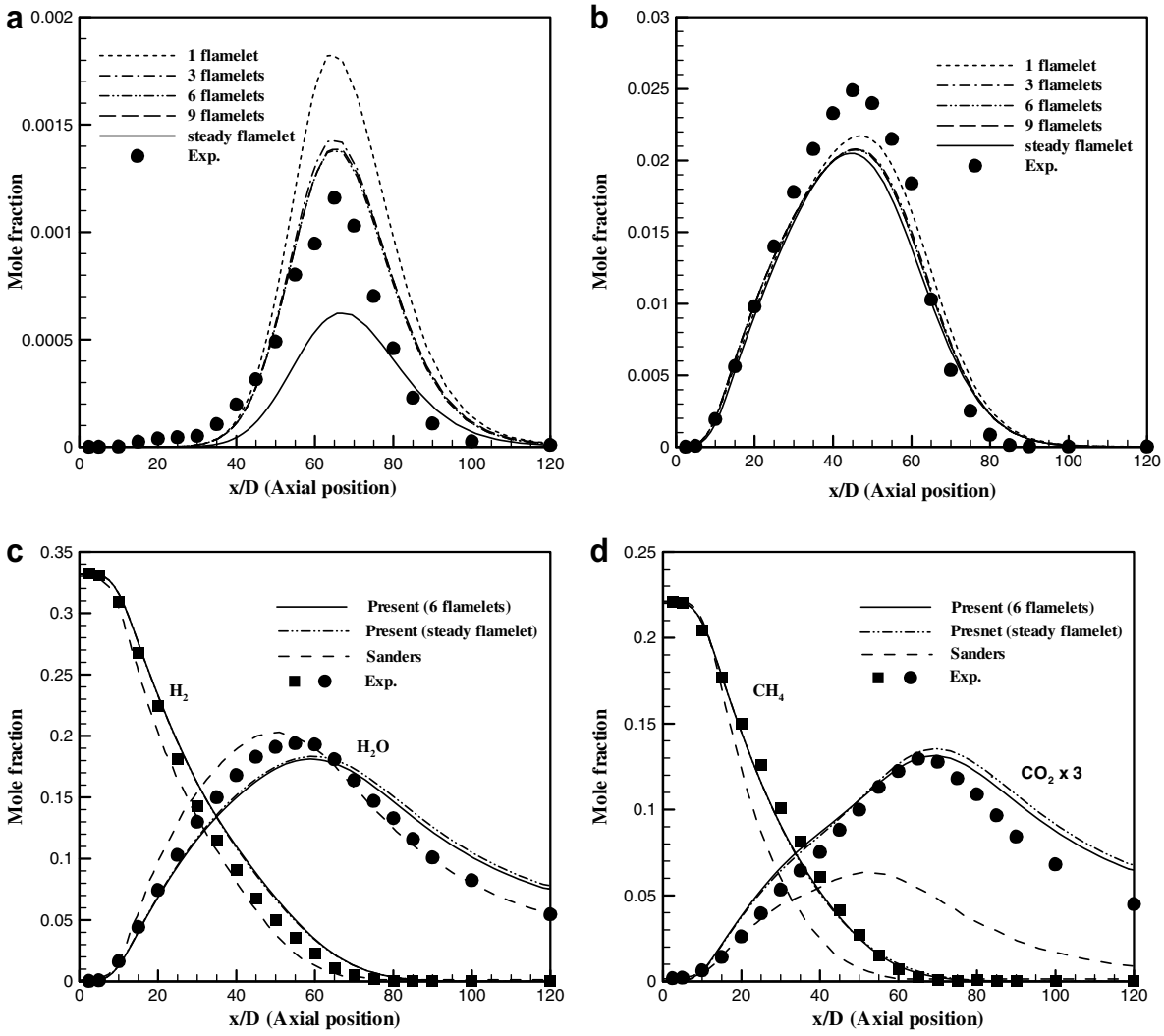

Fig. 3. Various species concentrations for steady and unsteady flamelet approaches: (a) OH, (b) CO, (c) H_2 and H_2O, and (d) CH_4 and CO_2.

ally in close agreement with the measured data. The CH_4 and CO_2 concentrations of the present calculation are seen to correlate much better with the data than those of Sanders'.

3.2. Analysis of NO in high temperature diluted air combustion

To examine the effects of air temperature and oxygen concentrations on the combustion characteristics and NO formation, a coaxial jet flame studied by Fujimori et al. [23] is considered. The schematic of the experimental setup is shown in Fig. 4(a), which was used to examine the effect of the liftoff height for highly preheated air with varying fuel flow rates on NO_x emission. Calculations are carried out for the flames attached to the nozzle. The methane of 373 K flows at a rate of 5.87×10^{-5} kg/s and the coflowing air at 7.03×10^{-3} kg/s. The air temperature is varied to be at 1273, 1373 and 1473 K and its oxygen concentration ranges from 16 to 4 vol%. The diluted air composition is given in Table 1.

To test the grid resolution, calculations were carried out with three different meshes, namely, 50×60, 70×80 and 90×100. The radial temperature distributions across two axial cross-sections, $x/D = 100$ and 300, are compared in Fig. 4(b). It is observed that the 70×80 mesh is sufficiently fine to resolve the flow field. The effects of the number of flamelet particles on NO concentrations in Fig. 4(c) show that the particle number of six is adequate for unsteady flamelet analysis. Therefore, the 70×80 mesh with six flamelet particles is used for these calculations.

The emission indices of NO_x ($NO + NO_2$) for two oxygen concentrations, diluted with nitrogen, are compared with the experimental data in Fig. 5. The index is defined as the amount of pollutant produced per unit mass of fuel by the combustion process:

$$\mathrm{EINO}_x\ (\mathrm{g/kg}) = \frac{W_{\mathrm{NO}_x} \int_V \dot{\omega}_{\mathrm{NO}_x}\,\mathrm{d}V}{-W_{\mathrm{CH}_4} \int_V \dot{\omega}_{\mathrm{CH}_4}\,\mathrm{d}V} \times 10^3$$

where W_{NO_x} and W_{CH_4} denote the molecular weights of NO_x and CH_4 while $\dot{\omega}_{\mathrm{NO}_x}$ and $\dot{\omega}_{\mathrm{CH}_4}$ the production rates (mol/m^3 s) of NO_x and CH_4, respectively. The 70×80 mesh, again, gives converged solution, which is in satisfactory agreement with the measured data. Despite the general agreement, the emission index is overpredicted when the oxygen concentration is 16%. Considering that the flame temperature increases with the oxygen concentration as shall be seen in Fig. 6, the thermal NO_x, and thus the total NO_x, may be overpredicted by the GRI 3.0 reaction mechanism when the temperature is high. The thermal NO_x portion of the total, plotted in the figure, indeed shows that the thermal route is increasingly the dominant NO_x producing mechanism as the temperature becomes high. This will be elaborated in more detail later in the paper.

The maximum flame temperature is plotted against the oxygen concentration in Fig. 6 for various inlet air temperatures. It

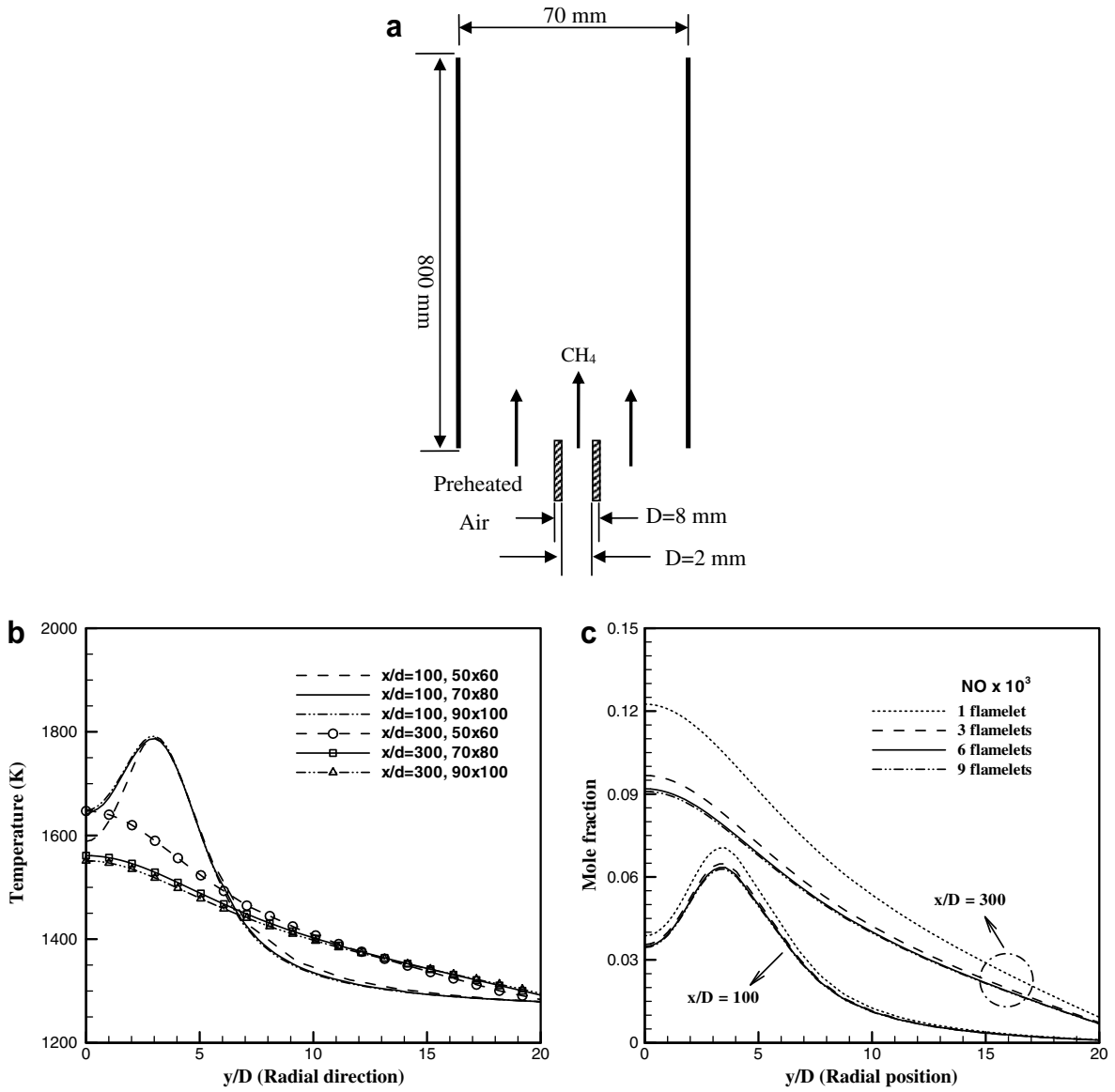

Fig. 4. Schematic of the experimental setup and effects of grid and number of particles on NO at inlet air of 1273 K and 10% O_2 concentration: (a) experimental setup, (b) temperature, and (c) NO.

Table 1
Composition of diluted air

Oxygen concentration (vol%)	Composition of diluted air (vol%)	
	Diluent: N_2	Diluent: CO_2
4	O_2(4):N_2(96)	O_2(4):N_2(15):CO_2(81)
8	O_2(8):N_2(92)	O_2(8):N_2(30):CO_2(62)
10	O_2(10):N_2(90)	O_2(10):N_2(38):CO_2(52)
12	O_2(12):N_2(88)	O_2(12):N_2(45):CO_2(43)
14	O_2(14):N_2(86)	O_2(14):N_2(53):CO_2(33)
16	O_2(16):N_2(84)	O_2(16):N_2(60):CO_2(24)

increases almost linearly with the oxygen concentration. The maximum flame temperature is higher for air diluted with nitrogen than that diluted with carbon dioxide. This is attributed to the difference in the heat capacity between the two diluents as noted in Yuan and Naruse [4]. The characteristics of the temperature distribution in the furnace are examined in Fig. 7. T_{max} is the maximum flame temperature of the cross-section in the axial direction while T_{mean} is the average temperature in the furnace. It is clear from the figure that the temperature tends to become more uniform as the oxygen concentration decreases. When the oxygen concentration is high, most of the reaction occurs near the fuel-nozzle exit and raises the temperature there. With less fuel available in the downstream region, the temperature is much lower than that in the upstream region. When the intake air is diluted, the reaction occurs more uniformly throughout the furnace and the temperature also becomes uniform. The air diluted with carbon dioxide provides more uniform temperature fields than that diluted with nitrogen.

The emission indices of NO for various air temperatures and oxygen concentrations are compared in Fig. 8. A lower oxygen concentration and/or a lower inlet air temperature yield a lower NO formation. For the air diluted with carbon dioxide, however, the effect of the inlet air temperature on the NO formation appears to be insignificant when the oxygen concentration is low, say less than 10%. The oxygen concentration above that value is seen to increase the emission index (EINO) almost exponentially. This is attributed to the temperature effects on the NO formation mechanism: the rate of thermal NO formation is known to be substantially high at a high flame temperature, say above 1800 K. When

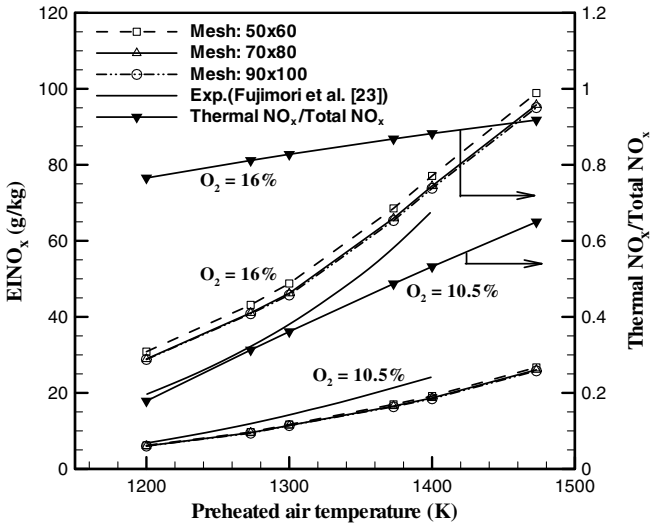

Fig. 5. Emission index of NO_x vs. inlet air temperature.

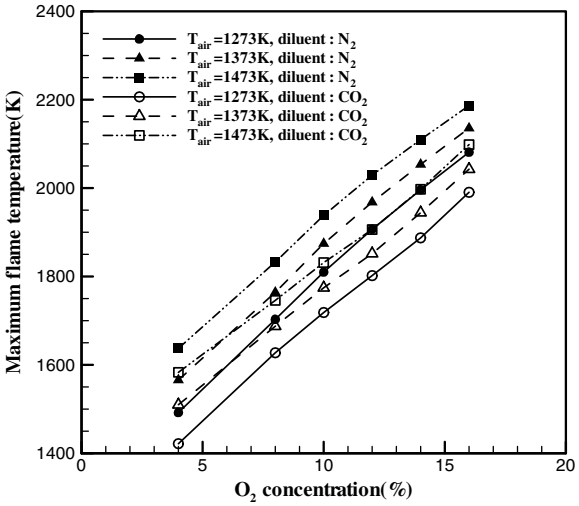

Fig. 6. Maximum flame temperature vs. oxygen concentration for various inlet air temperatures.

the oxygen concentration exceeds 12%, the maximum temperature attained in the region (Fig. 6) is seen to go over this value and the thermal route appears to be dominant in the NO formation. It is also observed from the figure that the air diluted with carbon dioxide results in much lower EINO than that with nitrogen.

It is well known that lowering the flame temperature reduces the NO formation by suppressing the thermal NO formation, however, various routes of NO formation have not been examined quantitatively in high temperature diluted air combustion. Many experiments and detailed kinetic calculations have been carried out to explore the formation mechanisms of nitric oxides [24,25]. NO is formed mainly through the thermal, prompt and N_2O intermediate routes. The formation of thermal NO is determined by a set of highly temperature dependent chemical reactions:

$$N + NO = N_2 + O \quad \text{(R178)}$$

$$N + O_2 = NO + O \quad \text{(R179)}$$

$$N + OH = NO + H \quad \text{(R180)}$$

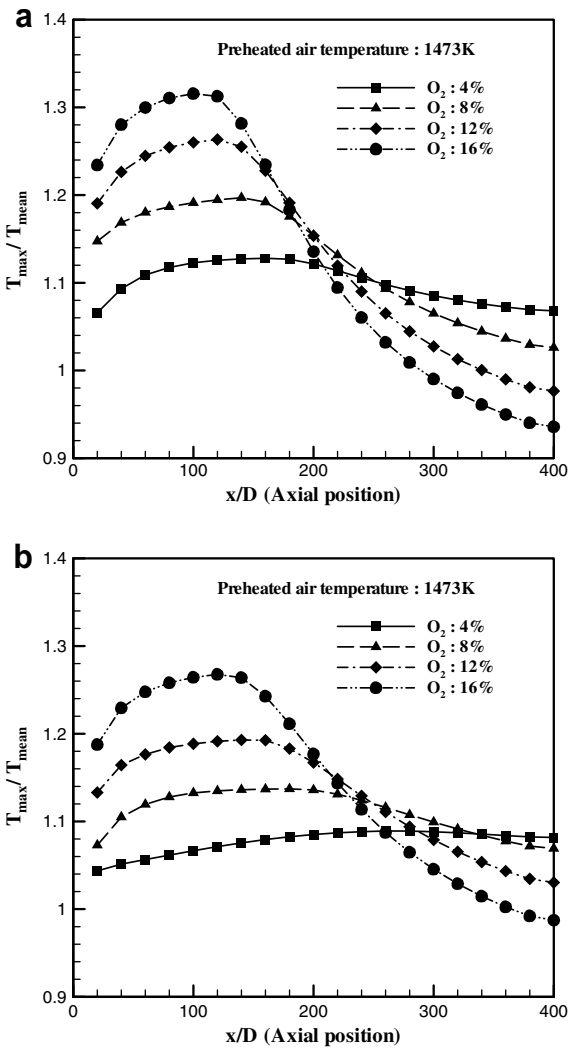

Fig. 7. Temperature distributions along the axis for various oxygen concentrations: (a) air diluted with N_2 and (b) air diluted with CO_2.

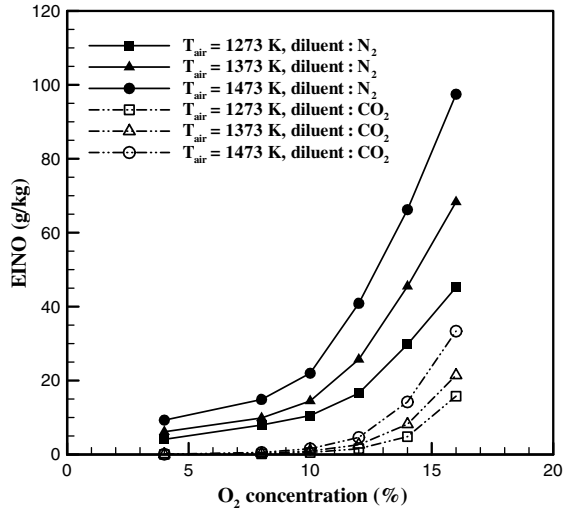

Fig. 8. EINO vs. oxygen concentration for various inlet air temperatures.

The N_2O intermediate mechanism becomes important in fuel lean and low temperature conditions. N_2O is mainly formed through Reaction (R185) and is converted to NO by Reactions (R199) and (R182)

$$N_2O + M = N_2 + O + M \quad (R185)$$

$$NH + NO = N_2O + H \quad (R199)$$

$$N_2O + O = 2NO \quad (R182)$$

The prompt NO in hydrocarbon flames is initiated by the rapid reaction of hydrocarbon radicals with molecular nitrogen

$$CH + N_2 = HCN + N \quad (R240)$$

The contributions of the thermal, prompt, and N_2O intermediate routes to the NO formation for various oxygen concentrations at the inlet air temperature of 1373 K are shown in Fig. 9. The N_2O intermediate route in this case appears to be relatively small compared to the other two routes, and thus will not be discussed here. As the oxygen concentration increases, the contribution by the thermal NO route becomes substantially higher than the other. When the oxygen concentration is higher than 14%, the increase in EINO is mainly caused by the thermal mechanism. If the oxygen concentration falls below 8%, EINO is reduced to a very low level; the prompt route is seen to be the major NO producing mechanism especially when the air is diluted with nitrogen. This may be better illustrated in Fig. 10 that shows the production rate of Reaction (R240) and the mole fraction of HCN along the centerline for two

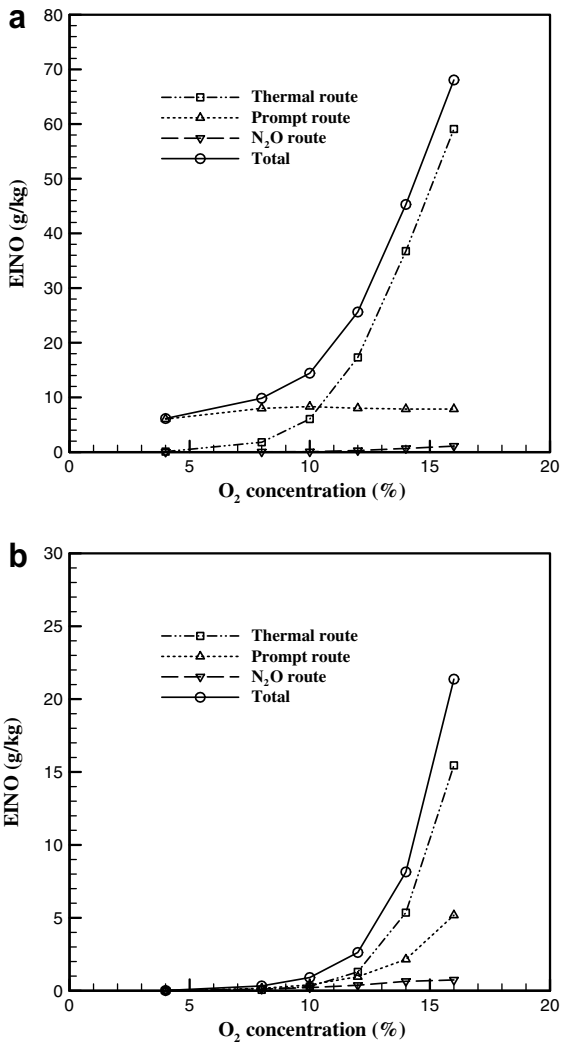

Fig. 9. Contributions of various NO formation routes at inlet temperature of 1373 K: (a) air diluted with N_2 and (b) air diluted with CO_2.

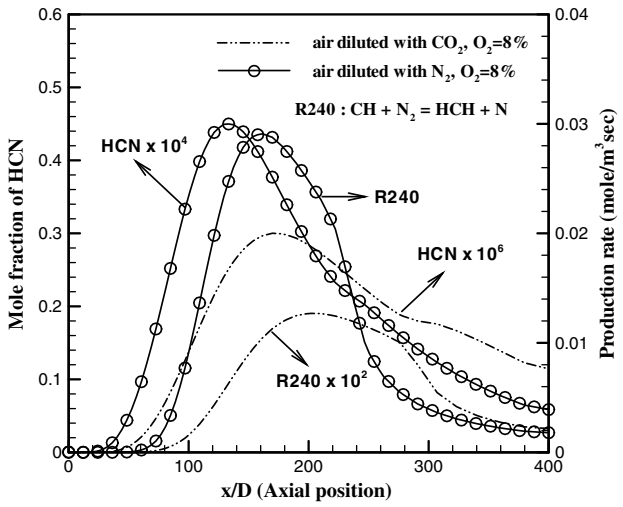

Fig. 10. Production rates and HCN concentration for inlet air of 8% oxygen and 1373 K.

different diluents with 8% oxygen. When the air is diluted with nitrogen, there are more nitrogen contents in the inlet air than that diluted with carbon dioxide. A higher nitrogen concentration obviously enhances Reaction (R240) and results in higher HCN production. As the amount of HCN dictates the NO formation in the prompt mechanism, the air dilution with nitrogen gives higher NO formation.

As seen above, the combustion characteristics differ as the diluent changes from CO_2 to N_2. The air dilution with carbon dioxide gives a lower maximum flame temperature and lower NO formation compared to the air dilution with nitrogen. This is a direct consequence of the difference in heat capacity, the product of the density and specific heat, between the two diluents [4]. In addition, the extra nitrogen content in the air contributes to NO formation through the prompt route. To see it more clearly, the results for two different oxygen concentrations are compared in Fig. 11. Fig. 11(a) shows the temperature and NO concentrations along the centerline. Although the temperature for the diluted air of 14% oxygen concentration with carbon dioxide is higher than that for the diluted air of 10% oxygen concentration with nitrogen, the former gives a lower NO concentration than the latter. This is explained by examining the various NO formation mechanisms in more detail. The thermal NO is produced mainly by the reactions $N_2 + O = N + NO$ and $N + OH = NO + H$. Also, the O and OH concentrations affect the thermal NO formation. The production rate of reaction $N_2 + O = N + NO$ and the OH concentration are plotted in Fig. 11(b). The diluted air of 14% oxygen with carbon dioxide gives higher production rate and concentration than the diluted air of 10% oxygen with nitrogen. Consequently, the 14% oxygen diluted with carbon dioxide gives higher thermal NO than 10% oxygen diluted with nitrogen. On the other hand, for the prompt NO route, the 10% oxygen diluted with nitrogen gives a much higher production rate than the 14% oxygen diluted with carbon dioxide. As a result, higher prompt NO is produced in the case of 10% oxygen diluted with nitrogen than the other as seen in Fig. 11(a). This makes the total NO formation higher as was mentioned above. Although the diluted air gives a lower NO formation by suppressing thermal NO, the NO formation by the prompt route is still significant especially when the air is diluted with nitrogen. For fuels with no nitrogen contents, NO is formed by oxidation of molecular nitrogen in the air. The amount of nitrogen in the

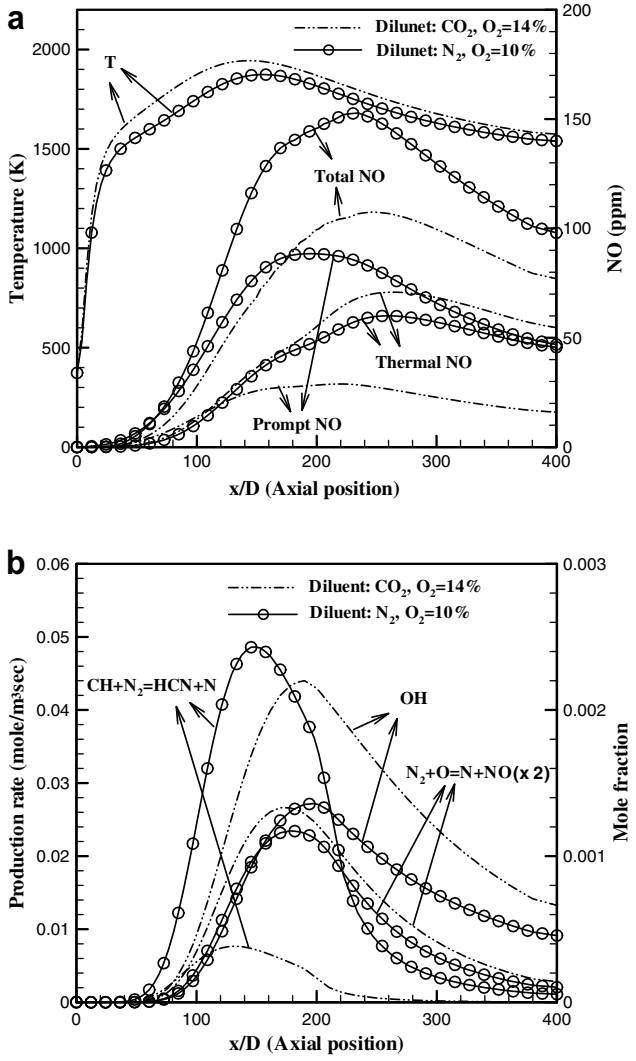

Fig. 11. Combustion characteristics for different diluents: (a) temperature and NO concentration and (b) production rates of Reactions (R178) and (R240) and OH concentration.

air plays a key role in the NO formation at low oxygen concentration.

4. Conclusions

The laminar flamelet model has been successfully incorporated in a finite volume method and applied to predict combustion characteristics in a coaxial jet flame. For accurate prediction of NO formation, the unsteady flamelets are calculated in a postprocessing mode by solving Eulerian particle transport equations. The essential characteristics of turbulent high temperature diluted air combustion in a coaxial jet flame are seen to be well captured. The carbon dioxide is a more effective diluent than the nitrogen in reducing the maximum temperature and NO formation. When the oxygen concentration is high, the NO formation is mostly affected by the thermal mechanism due to the flame temperature increase and the reaction zone is formed near the fuel nozzle. On the other hand, when the oxygen concentration is low, the reaction is not limited to upstream region and occurs more uniformly in the furnace. In particular, when the air is diluted with nitrogen, the NO formation by the prompt route is much more pronounced than other routes. Because the prompt NO in hydrocarbon flame is primarily formed by the rapid reactions of hydrocarbon radicals with molecular nitrogen, the amount of nitrogen in the inlet air greatly affects the NO formation at low oxygen concentration.

Acknowledgements

This work was supported by KOSEF through the Combustion Engineering Research Center at KAIST.

References

[1] A.K. Gupta, S. Bolz, T. Hasegawa, Effect of air preheated temperature and oxygen concentration on flame structure and emission, J. Energy Resour. Technol. 121 (1999) 209–216.
[2] S. Lille, W. Blasiak, M. Jewartowski, Experimental study of the fuel jet combustion in high temperature and low oxygen content exhaust gases, Energy 30 (2005) 373–384.
[3] M. Mortberg, W. Blasiak, A.K. Gupta, Combustion of normal and low calorific fuel in high temperature and oxygen deficient environment, Combust. Sci. Technol. 178 (2006) 1345–1372.
[4] J. Yuan, I. Naruse, Modeling of combustion characteristics and NO_x emission in highly preheated and diluted air combustion, Int. J. Energy Res. 22 (1998) 1217–1243.
[5] S. Orsino, R. Weber, Numerical simulation of combustion of natural gas with high-temperature air, Combust. Sci. Technol. 170 (2001) 1–34.
[6] W. Yang, W. Blasiak, Numerical study of fuel temperature influence on single gas jet combustion in highly preheated and oxygen deficient air, Energy 30 (2005) 385–398.
[7] T. Ishii, C. Zhang, S. Sugiyama, Numerical simulations of highly preheated air combustion in an industrial furnace, J. Energy Resour. Technol. 120 (1998) 276–284.
[8] W. Yang, W. Blasiak, Mathematical modeling of NO emissions from high-temperature air combustion with nitrous oxide mechanism, Fuel Proces. Technol. 86 (2005) 943–957.
[9] Y. Ju, T. Niioka, Computation of NO_x emission of a methane–air diffusion flame in a two-dimensional laminar jet with detailed chemistry, Combust. Theor. Model. 1 (1997) 243–258.
[10] N. Peters, Laminar diffusion flamelet models in non-premixed turbulent combustion, Prog. Energy Combust. Sci. 10 (1984) 319–339.
[11] H. Pitsch, M. Chen, N. Peters, Unsteady flamelet modeling of turbulent hydrogen–air diffusion flames, Proc. Combust. Inst. 27 (1998) 1057–1064.
[12] H. Barths, N. Peters, N. Brehm, A. Mack, M. Pfitzner, V. Smiljanovski, Simulation of pollutant formation in gas-turbine combustion using unsteady flamelets, Proc. Combust. Inst. 27 (1998) 1841–1847.
[13] P.J. Coelho, N. Peters, Numerical simulation of a mild combustion burner, Combust. Flame 124 (2001) 503–518.
[14] B. Marracino, D. Lentini, Radiation modeling in non-luminous non-premixed turbulent flames, Combust. Sci. Technol. 128 (1997) 23–48.
[15] H.S. Kim, S.W. Baek, M.J. Yu, Formation characteristics of nitric oxide in a three-staged air/LPG flame, Int. J. Heat Mass Transfer 46 (2003) 2993–3008.
[16] V. Bergmann, W. Meier, D. Wolff, W. Stricker, Application of spontaneous Raman and Rayleigh scattering and 2D LIF for the characterization of a turbulent $CH_4/H_2/N_2$ jet diffusion flame, Appl. Phys. B 66 (1998) 489–502.
[17] W. Meier, R.S. Barlow, Y.-L. Chen, J.-Y. Chen, Raman/Rayleigh/LIF measurements in a turbulent $CH_4/H_2/N_2$ jet diffusion flame: experimental techniques and turbulent–chemistry interaction, Combust. Flame 123 (2000) 326–343.
[18] R.J. Kee, R.M. Rupley, J.A. Miller, Chemkin-II: A Fortran chemical kinetics package for the analysis of gas-phase chemical kinetics, Sandia National Laboratories Report SAND 89-8009, 1989.
[19] R.J. Kee, J. Warnatz, J.A. Miller, A Fortran computer code package for the evaluation of gas-phase viscosities conductivities and diffusion coefficients, Sandia National Laboratories Report SAND 83-8209, 1983.
[20] R.S. Barlow, A.N. Karpetis, J.H. Frank, J.-Y. Chen, Scalar profiles and NO formation in laminar opposed-flow partially premixed methane/air flames, Combust. Flame 127 (2001) 2102–2118.
[21] T. Shimizu, F.A. Williams, Concentrations of nitric oxide in laminar counterflow methane/air diffusion flames, J. Propul. Power 21 (2005) 1019–1028.
[22] K.W. Lee, D.H. Choi, Prediction of NO in turbulent diffusion flames using Eulerian particle flamelet model, Combust. Theor. Model. 12 (2008) 905–927.
[23] T. Fujimori, D. Riechelmann, J. Sato, Effect of liftoff on NO_x emission of turbulent jet flame in high-temperature coflowing air, Proc. Combust. Inst. 27 (1998) 1149–1155.
[24] C.P. Fenimore, Formation of nitric oxide in premixed hydrocarbon flames, Proc. Combust. Inst. 13 (1970) 337–380.
[25] J.A. Miller, C.T. Bowman, Mechanism and modeling of nitrogen chemistry in combustion, Prog. Energy Combust. Sci. 15 (1989) 287–338.